A Pair of Twisted Jets of Ionized Iron from L 1551 IRS 5

Itoh, Yoichi ; Kaifu, Norio ; Hayashi, Masahiko ; Hayashi, Saeko S. ; Usuda, Tomonori ; Noumaru, Jun'ichi ; Maihara, Toshinori ; Iwamuro,…

(Citation)
Publications of the Astronomical Society of Japan,52(1):81-86

(Issue Date)
2000-02-25

(Resource Type)
journal article

(Version)
Version of Record

(URL)
https://hdl.handle.net/20.500.14094/90001439

PASJ: Publ. Astron. Soc. Japan **52**, 81–86 and Plate 18–19 (2000)

A Pair of Twisted Jets of Ionized Iron from L 1551 IRS 5

Yoichi ITOH, Norio KAIFU, Masahiko HAYASHI, Saeko S. HAYASHI,
Takuya YAMASHITA, Tomonori USUDA, Jun'ichi NOUMARU
Subaru Telescope, 650 North A'ohōkū Place, Hilo, HI 96720, U.S.A.
E-mail (YI): yitoh@subaru.naoj.org
and

Toshinori MAIHARA, Fumihide IWAMURO, Kentaro MOTOHARA,
Tomoyuki TAGUCHI, and Ryuji HATA
Department of Physics, Kyoto University, Sakyo-ku, Kyoto 606-8502

(Received 1999 November 1; accepted 1999 November 24)

Abstract

High-resolution near-infrared J-band imaging with the Subaru Telescope has demonstrated, for the first time from the ground, two independent jets emanating from the protostar L 1551 IRS 5. Successive near-infrared spectroscopy has revealed that the jet emission is dominated by [Fe II] lines in the J- and H-bands. While the visual-extinction estimated from the [Fe II] line ratios reaches more than 20 mag in the close vicinity of IRS 5, it decreases rapidly at $\sim 1''$ from IRS 5 and remains constant around 7 mag at larger distances. The electron density in the jets is estimated to be 10^6 cm^{-3} near IRS 5 and is 10^4 to 10^5 cm^{-3} in their outer section. The twisted appearance of the jets, with bright knots especially prominent in the northern jet, is similar to the R-band jets observed with the Hubble Space Telescope. These results suggest that the twisted structure and bright emission knots are intrinsic to the jets and are not due to a spatial variation of the extinction.

Key words: infrared: stars — ISM: jets and outflows — stars: formation

1. Introduction

L 1551 IRS 5 is one of the best-studied young stellar objects (YSOs) associated with an optical jet (Mundt, Fried 1983), a molecular outflow (Snell et al. 1980; Uchida et al. 1987), and Herbig–Haro objects (Davis et al. 1995; Hodapp, Ladd 1995). Recent high-resolution observations have revealed details of L 1551 IRS 5 (hereafter often referred to simply as IRS 5) and its close vicinity. VLA observations in various wavelength ranges discovered two thermal dust emission sources separated by ~ 40 AU from each other inside a larger disk of ~ 160 AU in diameter (Lay et al. 1994), suggesting a young binary system embedded in a circumbinary disk (Rodríguez et al. 1998). An infalling circumstellar envelope was found surrounding the binary system and the circumbinary disk with the Nobeyama Millimeter Array (Ohashi et al. 1996; Momose et al. 1998). At optical wavelengths, extensive studies have focused on the jet emanating from IRS 5. This jet was considered to have several knots in a wiggly pattern (Scarrott 1988), with the knots changing their positions and shapes over a period of decades (Neckel, Staude 1987; Campbell et al. 1988; Fridlund, Liseau 1994). High-resolution observations have revealed two rows of knots, which have been interpreted as a structure caused by the precession of a single jet (Campbell et al. 1988; Fridlund, Liseau 1994) or the limb-brightening of a single jet (Mundt et al. 1991). Recently, however, Hubble Space Telescope (HST) observations have resolved the 'jet' into two separate features showing different velocities and velocity gradients, suggesting that there are two independent jets, possibly arising from each star of the binary system (Fridlund, Liseau 1998, hereafter FL 98).

In this paper we discuss a near-infrared imaging and spectroscopic study of L 1551 IRS 5, carried out as part of first light observations with the Subaru Telescope. Thanks to the high imaging performance of the telescope, the two jets, emitting strong infrared [Fe II] lines, were clearly resolved for the first time from the ground. The jets share similar characteristics with the optical HST image in their twisted shape, implying thatthe twisted and knotty structure is intrinsic to the jets. We discuss the nature of the jets.

2. Observations

Near-infrared imaging observations of L 1551 IRS 5 were carried out on 1999 January 14 using the Subaru Telescope at the summit of Mauna Kea, with the infrared camera CISCO (Motohara et al. 1999) mounted

Table 1. Flux of the lines.*

ID	Slit position†	Object	Jet position‡	[Fe II] 12566 Å	[Fe II] 12785	[Fe II] 12942	[Fe II] 13205	[Fe II] 15334	[Fe II] 15995	[Fe II] 16435	[Fe II] 16769
A	+0.″1	Cont.	···	3.8 (0.8)	···	···	···	···	···	21.7 (1.1)	···
B	−0.6	Cont. and jet	0.″	26.4 (1.0)	···	···	9.4 (1.4)	25.8 (4.4)	···	110.6 (3.3)	···
C	−1.1	Cont. and jet	0.2	69.3 (1.8)	···	···	38.1 (4.2)	38.8 (1.4)	···	103.9 (7.6)	···
D	−1.6	Cont. and jet	0.4	41.0 (1.9)	···	···	33.4 (5.4)	22.1 (1.2)	21.2 (2.5)	61.3 (2.4)	···
Ea	−2.4	Cont.	1.1	···	···	···	···	···	···	15.6 (3.0)	···
Eb	−2.4	Jet(N)	2.3	70.2 (4.6)	13.2 (5.2)	19.2 (1.6)	25.5 (2.1)	20.7 (1.1)	13.0 (1.7)	112.3 (1.9)	13.7 (1.7)
Ec	−2.4	Jet(S)	···	29.2 (4.1)	···	···	···	···	···	45.2 (4.5)	···
Fa	−2.7	Cont.	···	···	···	···	···	···	···	9.0 (3.4)	···
Fb	−2.7	Jet(N)	···	95.8 (2.0)	···	···	40.5 (3.8)	27.2 (1.7)	23.0 (3.1)	127.8 (4.0)	19.1 (3.6)
Fc	−2.7	Jet(S)	···	20.1 (6.4)	···	···	···	···	···	24.2 (2.9)	···
Ga	−4.0	Jet(N)	···	67.1 (3.9)	···	···	20.1 (0.7)	22.1 (7.1)	20.5 (4.7)	92.3 (4.4)	9.3 (4.2)
Gb	−4.0	Jet(S)	···	17.7 (5.4)	···	···	···	···	···	31.5 (2.2)	···
Ha	−4.3	Jet(N)	···	23.1 (1.0)	···	···	5.8 (1.4)	···	···	36.3 (3.0)	···
Hb	−4.3	Jet(S)	···	19.9 (5.0)	···	···	7.6 (3.9)	···	···	35.5 (2.3)	···
Ia	−7.1	Jet(N)	···	25.1 (8.8)	···	···	···	···	···	35.7 (2.0)	···
Ib	−7.1	Jet(S)	···	21.6 (2.3)	···	···	···	···	···	29.0 (3.5)	···

*Unit of flux is arbitrary. Uncertainties are in parentheses.
†Slit position, + as east, − as west.
‡Jet position measured from the continuum, direction to south.

at the F/12 Cassegrain focus. CISCO is equipped with a 1024 × 1024 pixel HgCdTe array with a pixel scale of 0.″116 pixel^{-1}, providing a total field of view of 118″ square. Under a seeing condition of typically 0.″4 (FWHM), sixteen exposures of 10 s each were obtained at the J-band, and fifteen exposures of 0.5 s each at the K' (2.13 μm) band. Data reduction was performed with the IRAF packages. The flat-field frames for the J and K' images were constructed from median-filtered images of the corresponding sky frames.

The J- and H-band spectra were obtained on 1999 February 28 with the Subaru telescope utilizing the JH-grism spectroscopy mode of CISCO, which provided a spectral resolution of $\sim$ 280 at 1.4 μm. Typical FWHM of the point-spread function was again 0.″4 throughout the observations. A 1″ width slit, aligned north-south, was used, and IRS 5 was observed at 9 positions with 15″ dithering along the declination to provide sky subtraction. The 9 slit positions are shown in figure 1 (Plate 18). Note that the slit covered both (northern and southern) jets in the outer section. Three exposures of 20 s each were made at each slit position. We took a J-band image before setting the grism in the CISCO optics, to ensure correct placement of the slit. The slit was first set at the eastern-most position (spectrum ID = A), shown in figure 1 (Plate 18). A significant drift of the telescope pointing was determined, with successive spectra being taken further to the east of slit position A. The relative slit positions of the second, third, and forth spectra (IDs = B, C, and D), with respect to the eastern-most position, were determined from their J-band fluxes. The relative slit positions for the remaining five spectra (E–I) were not determined and have positional uncertainties of 0.″8, i.e., the pointing uncertainty of the telescope. The absolute slit positions were calibrated relative to the centroid of the IRS 5 radio continuum sources at $\alpha(2000) = 4^{h}28^{m}40^{s}.242$, $\delta(2000) = +18°01'42''.09$, 41.″77 (Rodríguez et al. 1998) by taking the RA offset of the J-band peak to be 0.″87 west with respect to the continuum source. This value was derived by averaging 1.″1 and 0.″8, which are the offsets of the z and H-band peaks, respectively, to the centroid of the radio continuum sources (Campbell et al. 1988; Hodapp et al. 1988), and by projecting the mean offset onto the RA axis. The overall uncertainty for the absolute slit positions is therefore $\sim$ 0.″15. SAO 93986 (A3 V) was used as a standard star for spectral calibration.

Flat-field frames for the spectral data were made from median-filtered images of the J-band sky frames. OH lines in the sky portion in each spectrum were used for wavelength calibration, and the resultant wavelength uncertainty was 8 Å rms. The standard star spectrum contained absorption lines of the Brackett series in the H-band; they were interpolated and removed. The object spectra were divided by the standard star spectrum and were multiplied by a blackbody spectrum representing the standard star. Fluxes of the emission lines were computed using the SPLOT task of IRAF. The uncertainty in the continuum level subtraction determined the line-flux uncertainty. The parameters and results of spectroscopy are tabulated in table 1.

3. Results and Discussion

3.1. Two Jets of Ionized Iron

Figure 1 (Plate 18) shows a composite J and K' image of the 60″× 80″ region around IRS 5. The two jets are clearly separated from and parallel to each other, with

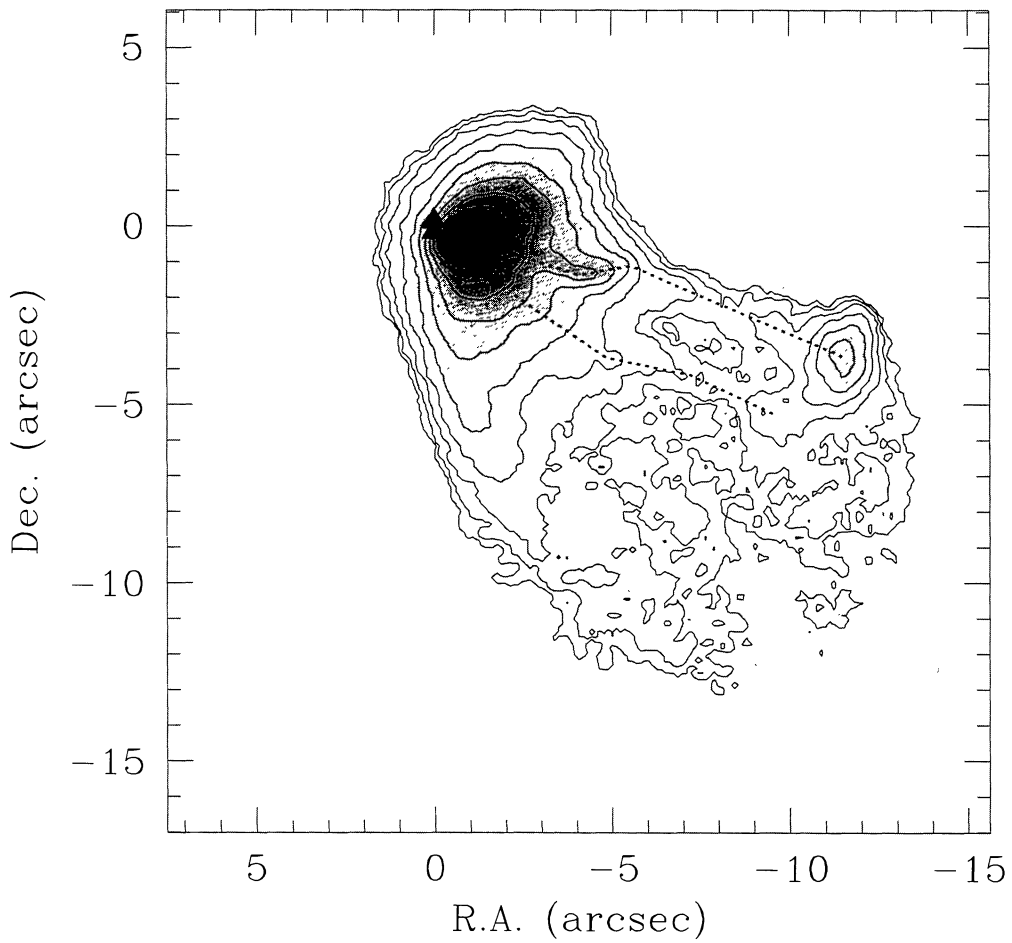

Fig. 3. J-band contour map of L 1551 IRS 5. The positions of compact radio continuum sources IRS 5 are shown by filled triangles. The peak-intensity positions along two jets are traced by dotted lines. Contour lines are drawn at relative intensities of $36 + 5.6 \times 10^{i/4}$ $(i = 0, 1, 2, \cdots)$.

both jets disappearing at $\sim 10''$ from IRS 5 (1400 AU for the assumed distance of 140 pc to L 1551). At this position the northern jet is terminated with a bright knot called "D" (Neckel, Staude 1987), while the southern jet smoothly disappears. Both jets have a similar brightness at 5″–9″ away from IRS 5, whereas the northern jet is stronger at knot D as well as in the region closer to IRS 5.

In order to see the jet morphology in more detail, we show the J-band image of the central $23''$ region in log scale [figure 2 (Plate 19)], as well as a contour presentation of the J-band image in figure 3. On the contour plot the peak positions along each jet are traced. While the two jets are relatively straight and parallel to each other at positions more than $4''$ away from IRS 5, they change flow directions in the inner section and converge on a compact region, where two sources were discovered emitting a thermal dust continuum (Rodríguez et al. 1998). The northern jet is ejected along a position angle (PA) of 254° near to the origin, changing its direction slightly to the north with PA = 280° at a distance of 4.″3, and then turning to the south with PA = 247° at a distance of 5.″7. The southern jet, on the other hand, is initially ejected toward the southwest with PA = 233°, making a change of direction to the north with PA = 258° at 6.″0, and turning to PA = 245° at 8.″2 from IRS 5.

Figure 4 shows the J-band contours superimposed on the HST R-band image (FL 98). The jets in the J-band show basically the same morphological characteristics as those in the R-band. It is remarkable, in particular, that each of the R-band emission knots seen predominantly in the northern jet has corresponding J-band emission. Except for the innermost knot of the northern jet ($< 4''$ from IRS 5), the brightness ratio of the knots relative to the quiescent portion of the jet is ~ 2 in the R-band, which is larger than the J-band ratio of ~ 1.3. This fact makes the northern jet, having many of knots, apparently

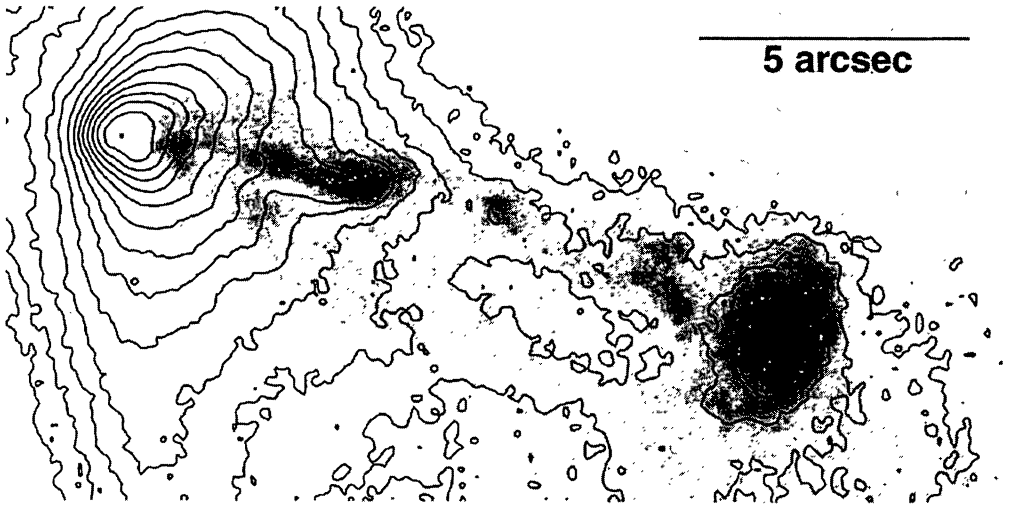

Fig. 4. J-band contour map superimposed on the R-band HST image (FL 98). The field of view is $17'' \times 8\farcs5$. North is up, and east is toward the left.

Table 2. Flux ratio of the lines, extinctions, and electron densities.

ID	$\frac{I_{164}}{I_{125}}$	$\frac{I_{153}}{I_{164}}$*	$\frac{I_{153}}{I_{125}}$*	A_V	log N_e(164/153)	log N_e(153/125)
A	$5.75^{+1.31}_{-0.96}$	...	...	$21.9^{+2.2}_{-2.0}$	...	...
B.....	$4.19^{+0.21}_{-0.19}$	$0.26^{+0.04}_{-0.03}$	$0.68^{+0.10}_{-0.10}$	$18.5^{+0.5}_{-0.5}$	4.4±0.2	>6
C.....	$1.50^{+0.11}_{-0.10}$	$0.42^{+0.03}_{-0.03}$	$0.39^{+0.02}_{-0.02}$	$7.6^{+0.73}_{-0.76}$	>5.6 (10000 K, 12000 K)	>6
D	$1.50^{+0.09}_{-0.09}$	$0.40^{+0.03}_{-0.02}$	$0.37^{+0.03}_{-0.02}$	$7.5^{+0.7}_{-0.6}$	>5.4 (10000 K, 12000 K)	>6
Eb	$1.60^{+0.10}_{-0.09}$	$0.21^{+0.01}_{-0.01}$	$0.20^{+0.02}_{-0.01}$	$8.2^{+0.6}_{-0.6}$	4.05±0.05	4.7±0.1
Ec.....	$1.55^{+0.29}_{-0.24}$	...	...	$7.9^{+1.9}_{-1.8}$	...	...
Fb	$1.33^{+0.05}_{-0.05}$	$0.24^{+0.02}_{-0.02}$	$0.20^{+0.01}_{-0.01}$	$6.3^{+0.4}_{-0.4}$	4.2±0.2	4.7±0.1
Fc.....	$1.20^{+0.49}_{-0.30}$	...	...	$5.2^{+3.6}_{-3.2}$	...	...
Ga	$1.38^{+0.10}_{-0.10}$	$0.27^{+0.07}_{-0.07}$	$0.23^{+0.06}_{-0.06}$	$6.6^{+0.8}_{-0.8}$	4.4±0.4 or > 6 (3000 K)	4.7-0.3 or > 6
Gb	$1.78^{+0.60}_{-0.39}$	...	...	$9.4^{+3.1}_{-2.6}$	...	...
Ha	$1.57^{+0.15}_{-0.13}$	...	...	$8.1^{+0.9}_{-1.0}$	...	...
Hb	$1.78^{+0.48}_{-0.34}$	...	...	$9.4^{+2.6}_{-2.2}$		
Ia	$1.42^{+0.55}_{-0.33}$	...	...	$7.0^{+3.5}_{-2.8}$		
Ib	$1.34^{+0.23}_{-0.20}$	...	...	$6.3^{+1.7}_{-1.7}$		

*Extinction corrected.

brighter as a whole than the southern jet in the R-band. FL 98 argued that the northern jet is a currently active one, whereas the southern jet may be a fossil remnant of an outflow active in the past. The J-band image shows, however, that both the northern and southern jets have similar brightness, except for the knots, implying that both jets may be currently active.

Figure 5 shows a JH-grism spectrum of the northern jet at slit position E, which is $2\farcs4$ west of the radio continuum source along the northern jet. Most of the spectral features are identified as [Fe II] emission lines, as indicated in the figure, suggesting that the jets are predominantly bright in the [Fe II] lines. The [Fe II] line fluxes listed in table 1 indicate that the emission lines are more than 3-times stronger in the northern jet than in the southern jet within $4''$ of IRS 5. The jets show simi-

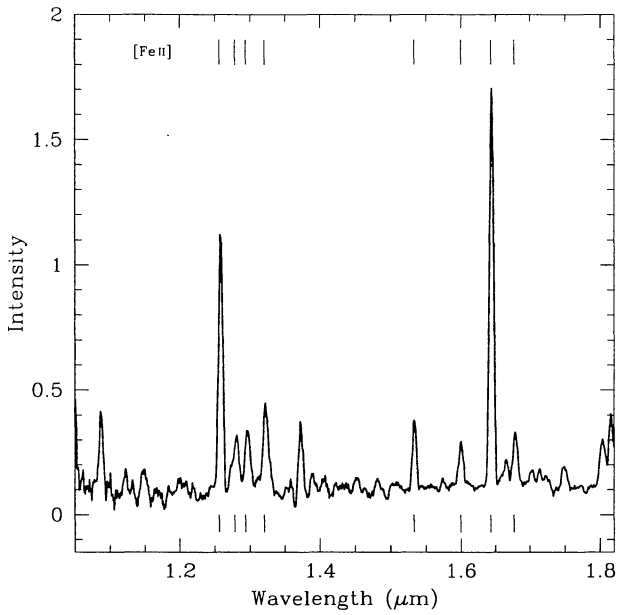

Fig. 5. JH-band spectrum of the northern jets (spectrum ID = Eb). The wavelength of the [Fe II] lines are shown by bars at the top and bottom of the figure.

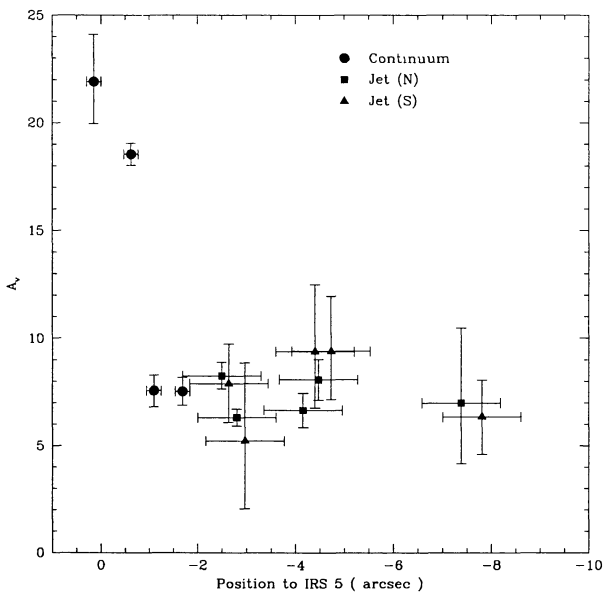

Fig. 6. Visual extinction estimated from the line ratios of the [Fe II] lines. The positions are measured in the direction of the jets.

lar [Fe II] line fluxes at slit position I (7″ west of IRS 5), consistent with the apparently similar J-band brightness of the two jets around this position, as mentioned above.

3.2. *Extinction and Electron Density*

We list in table 2 the visual extinction and electron density determined at each slit position. The extinction to the jets was estimated from the flux ratio of the [Fe II] 1.644 μm/1.257 μm lines, assuming an intrinsic ratio of 0.74 (Nussbaumer, Storey 1988). We then calculated the electron density of the jets from the extinction-corrected [Fe II] 1.257, 1.533, and 1.644 μm line fluxes (Nussbaumer, Storey 1988; Pradhan, Zhang 1993). These line ratios are sensitive diagnostics to the electron density between 3×10^2 and 3×10^5 cm^{-3} with little dependence on the electron temperature (Hamman et al. 1994, and references therein).

The spatial variation of visual extinction toward the jets is shown in figure 6. The extinction rapidly decreases beyond 1″ from IRS 5. A maximum visual extinction of 22 mag was observed toward the center of IRS 5, and is consistent with the previous measurements of extinction to this object (Ladd et al. 1995; Fuller et al. 1995). The high extinction toward of IRS 5 and its rapid decrease at a distance of 1″ may suggest that the compact dust disk (Lay et al. 1994) or the inner part of the infalling gas disk (Ohashi et al. 1996; Momose et al. 1998) is responsible for the localized extinction, since their projected radii on the jet direction have a size comparable to that of the high-extinction region.

The extinction in the outer section (more than 1″ away from IRS 5) is around 7 mag, and is constant within the measurement uncertainties (typically 3 mag). This again demonstrates that the brightness variation and twisted structure of the jets is not due to inhomogeneities in the circumstellar matter distribution, but is intrinsic to the jets.

The electron density in the jets is plotted against the distance from IRS 5 in figure 7. It is 10^4–10^5 cm^{-3} in their outer section, where it does not show a large variation, given the uncertainties. It may tend to increase to $\sim 10^6$ cm^{-3} within 2″ from IRS 5, although the large uncertainties seen in figure 7 prevent us from reaching a definite conclusion about the spatial density variation in the jets. The derived density is higher than that estimated from the optical [S II] lines (FL 98). This may be because the [S II] line ratio is sensitive to the electron density between 10^2 cm^{-3} and 10^4 cm^{-3}, which is 10-times lower than the sensitive range of [Fe II].

3.3. *The Twisted Structure*

The similarities in the morphology between the J- and R-band jets, together with the relatively homogeneous extinction toward them, affords evidence that the twisted pattern and knotty appearance is intrinsic to the jets. It

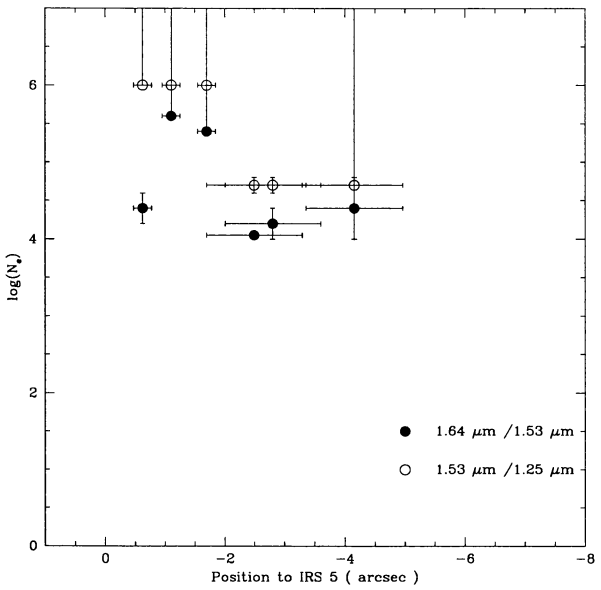

Fig. 7. Electron density estimated from the line ratios of the [Fe II]

may not be straightforward, however, to understand the physical mechanism responsible for such a zigzag structure.

The precession of the driving stars is often invoked as the cause of such wiggly patterns observed in galactic and extragalactic objects (Terquem et al. 1999). It may be difficult to apply the to the present case, however, when we consider the dynamical time scales. The time scale of the jets is $\sim$ 30 yr if we assume a jet speed of 300 km s^{-1}. The precession time scale, if the twisted pattern is produced by precession, might thus have a time scale of $\sim$ 10 yr, which is more than an order of magnitude smaller than the orbital period of $\sim$ 250 yr for a binary system of 0.5 $M_\odot$ stars separated by 40 AU It is difficult to make a dynamical model with such a short precession period. Moreover, the jet appearance is not sinusoidal either, which we would expect if periodic precession is the main cause of the zigzag pattern.

Magnetic fields may provide an alternative mechanism for producing wiggly jets. Each jet may originally be ejected along the polar axis of each star, but changes its direction to be aligned with the ambient magnetic field when the kinetic energy density of the jets, which may gradually decrease with distance from IRS 5 due to expansion, becomes comparable to the energy density of the ambient magnetic field. The bend at a distance of $\sim 4''$ seen in both jets might correspond to such a place. In this case the twisted jet pattern is stationary and is unchanged on a time scale longer than the dynamical time scale. In fact the [S II] image of the L 1551 jet obtained on 1986 Dec 31 (Mundt et al. 1991) has a knot which appears to correspond to the innermost bright part of the northern jet in our image, suggesting that the bright part of the jet existed more than 10 years ago. It may therefore be interesting to monitor the time variation of the twisted pattern to obtain a true understanding of its mechanism.

We are grateful to Drs. Luis Rodríguez, Alan Tokunaga, and Hiroshi Kinoshita for fruitful discussions. We thank Dr. Chris Simpson for reading the manuscript.

References

Campbell B., Persson S.E., Strom S.E., Grasdalen G.L. 1988, AJ 95, 1173
Davis C.J., Mundt R., Eislöffel J., Ray T.P. 1995, AJ 110, 766
Fridlund C.V.M., Liseau R. 1994, A&Ap 292, 631
Fridlund C.V.M., Liseau R. 1998, ApJ 499, L75 (FL 98)
Fuller G.A., Ladd E.F., Padman R., Myers P.C., Adams F.C. 1995, ApJ 454, 862
Hamann F., Simon M., Carr J.S., Prato L. 1994, ApJ 436, 292
Hodapp K.-W., Capps R.W., Strom S.E., Salas L., Grasdalen G.L. 1988, ApJ 335, 814
Hodapp K.-W., Ladd E.F. 1995, ApJ 453, 715
Ladd E.F., Fuller G.A., Padman R., Myers P.C., Adams F.C. 1995, ApJ 439, 771
Lay O.P., Carlstrom J.E., Hills R.E., Phillips T.G. 1994, ApJ 434, L75
Momose M., Ohashi N., Kawabe R., Nakano T., Hayashi M. 1998, ApJ 504, 314
Motohara K., Maihara T., Iwamuro F., Oya S., Imanishi M., Terada H., Goto M., Iwai J. et al. 1998, Proc. SPIE 3354, 659
Mundt R., Fried J.W. 1983, ApJ 274, L83
Mundt R., Ray T.P., Raga A.C. 1991, A&A 252, 740
Neckel Th., Staude H.J. 1987, ApJ 322, L27
Nussbaumer H., Storey P.J. 1988, A&A 193, 327
Ohashi N., Hayashi M., Ho P.T.P., Momose M., Hirano N. 1996, ApJ 466, 957
Pradhan A.K., Zhang H.L. 1993, ApJ 409, L77
Rodríguez L.F., D'Alessio P., Wilner D.J., Ho P.T.P., Torrelles J.M., Curiel S., Gómez Y., Lizano S. et al. 1998, Nature 395, 355
Scarrott S.M. 1988, MNRAS 231, 39
Snell R.L., Loren R.B., Plambeck R.L. 1980, ApJ 239, L17
Terquem C., Eislöffel J., Papaloizou J.C.B., Nelson R.P. 1999, ApJ 512, L131
Uchida Y., Kaifu N., Shibata K., Hayashi S.S., Hasegawa T., Hamatake H. 1987, PASJ 39, 907

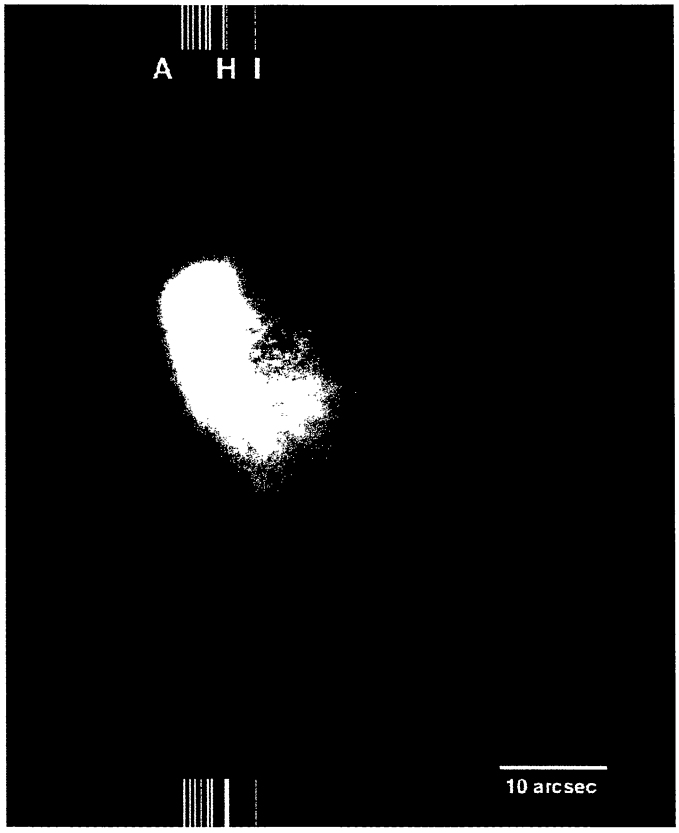

Fig. 1. Pseudo-colored near-infrared image of L 1551 IRS 5. The field of view is about $60'' \times 80''$. The J-band emission is registered as green, and K' as red, respectively. The slit positions of the spectroscopic measurement are indicated at the top and bottom of the image by yellow bars. North is up, and east is toward the left.

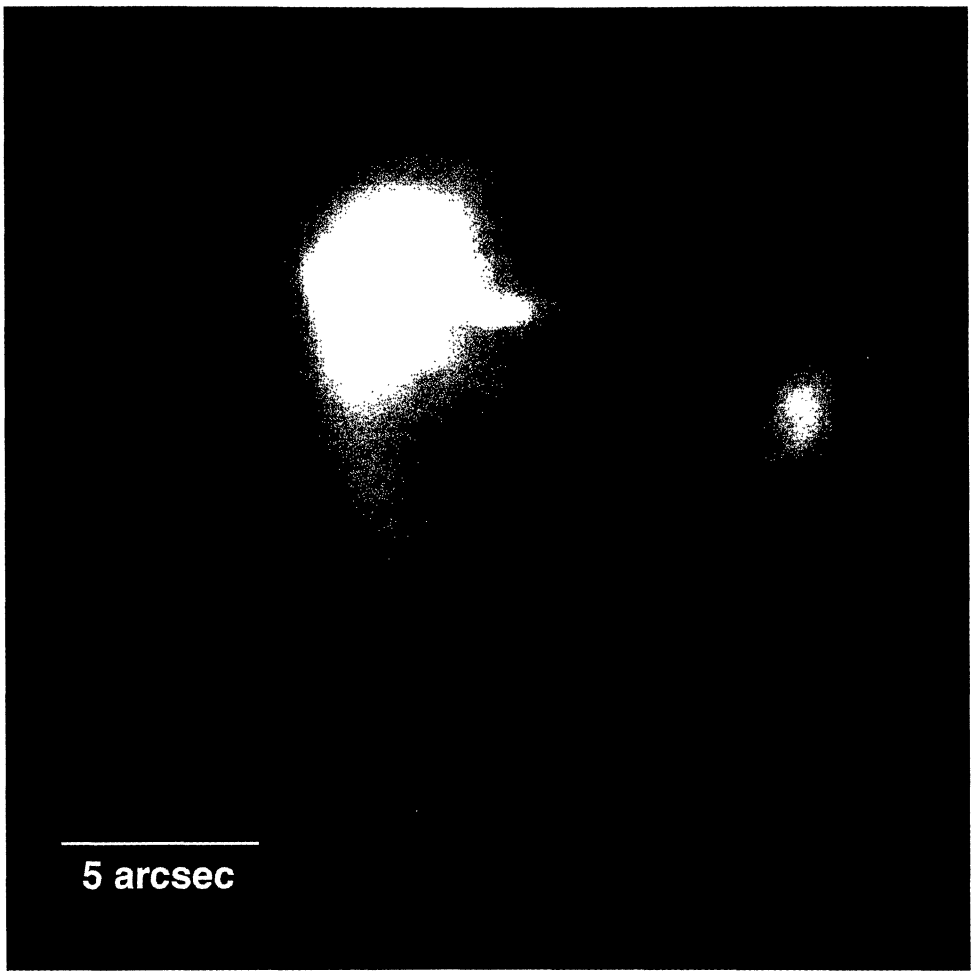

Fig. 2. J-band image of L 1551 IRS 5. The field of view is $23'' \times 23''$. A logarithmic intensity transfer table was used. North is up, and east is toward the left.